Provided for non-commercial research and education use.
Not for reproduction, distribution or commercial use.

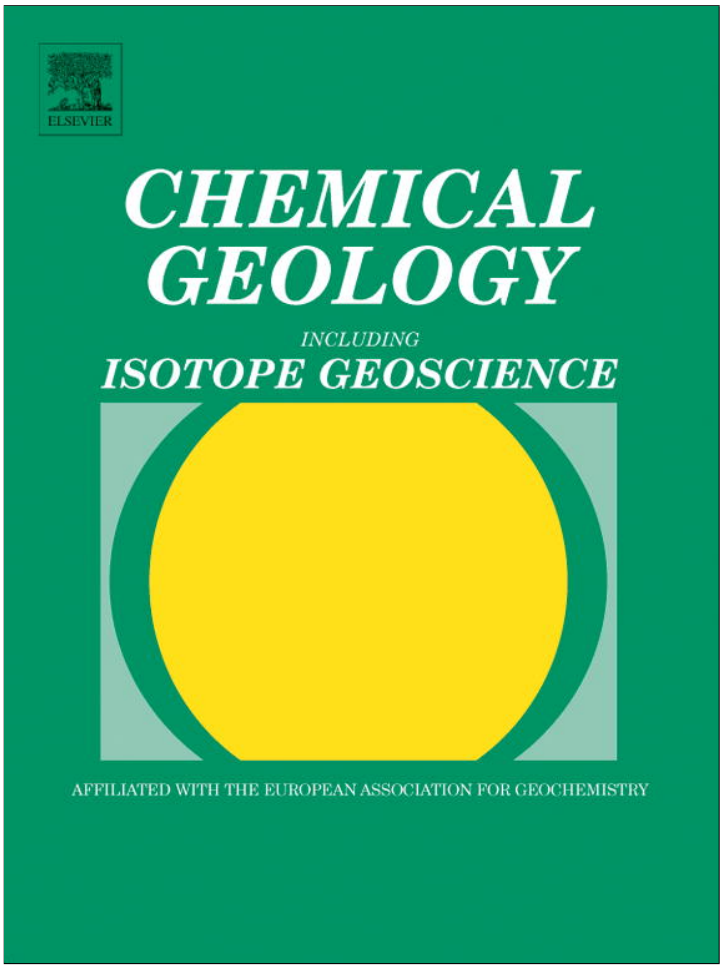

(This is a sample cover image for this issue. The actual cover is not yet available at this time.)

This article appeared in a journal published by Elsevier. The attached copy is furnished to the author for internal non-commercial research and education use, including for instruction at the authors institution and sharing with colleagues.

Other uses, including reproduction and distribution, or selling or licensing copies, or posting to personal, institutional or third party websites are prohibited.

In most cases authors are permitted to post their version of the article (e.g. in Word or Tex form) to their personal website or institutional repository. Authors requiring further information regarding Elsevier's archiving and manuscript policies are encouraged to visit:

http://www.elsevier.com/copyright

Author's personal copy

Chemical Geology 337-338 (2013) 88–98

Contents lists available at SciVerse ScienceDirect

Chemical Geology

journal homepage: www.elsevier.com/locate/chemgeo

Assessing the control on the effective kinetic Cr isotope fractionation factor: A reactive transport modeling approach

Christoph Wanner *, Eric L. Sonnenthal

Lawrence Berkeley National Laboratory, 1 Cyclotron Road, Berkeley, CA 94720, United States

ARTICLE INFO

Article history:
Received 4 April 2012
Received in revised form 2 November 2012
Accepted 17 November 2012
Available online 27 November 2012

Editor: B. Sherwood Lollar

Keywords:
Cr(VI) reduction
Cr isotope fractionation
Cr isotope fractionation factor
Reactive transport modeling
Transport limitations
Reaction mechanism

ABSTRACT

The fractionation of stable Cr isotopes is a well-accepted proxy for demonstrating Cr(VI) reduction occurring in geological systems. Published values for experimentally determined effective kinetic Cr isotope enrichment factors (ε_{kin}) vary over the range of 0.4–5.0‰. Most published studies propose a variation in Cr(VI) reduction mechanisms as being responsible for the wide range of ε_{kin}. Alternatively, varying reaction rates and/or transport limitations have been addressed. In this study the different contributions on ε_{kin} were quantitatively addressed by performing a series of reactive transport model simulations. The proposed reaction network is based on a novel multi-continuum approach and expressing isotope fractionation through the formation of a $^{53}Cr(OH)_{3(s)}$–$^{52}Cr(OH)_{3(s)}$ solid solution as the product of Cr(VI) reduction. In doing so, Cr(VI) reduction was considered to occur at solid surfaces and Cr isotope fractionation was modeled by defining an equilibrium enrichment factor.

Simulating Cr(VI) reduction occurring along a 1D flow path suggested that for a given reaction mechanism ε_{kin} can vary over a large range. According to our simulations the upper range of ε_{kin} is defined by a reaction mechanism's theoretical equilibrium enrichment factor. In contrast, high reduction rate and/or transport limitations can shift ε_{kin} to very low values. In a second model simulation our modeling approach was used to propose an alternative kinetic interpretation for the low ε_{kin} observed in Fe(II)–Cr(VI) reduction experiment by others. Our simulations suggest that the individual contributions of reaction rates, transport limitations and reaction mechanisms should be addressed more carefully when interpreting experimentally determined kinetic Cr isotope enrichment factors and Cr isotope data derived from field sites. Reactive transport modeling is a powerful tool, which should be more commonly used to quantitatively assess these individual contributions in experimental systems.

© 2012 Elsevier B.V. All rights reserved.

1. Introduction

In nature, Cr mostly occurs in two stable oxidation states. The highly toxic and very soluble oxidized form Cr(VI) is primarily derived from anthropogenic activities such as leather tanning, wood impregnation, galvanization of metal surfaces and cement clinker. Cr(VI) occurs as the chromate oxyanions CrO_4^{2-}, $HCrO_4^-$ and $Cr_2O_7^{2-}$ and can lead to health problems such as lung cancer and dermatitis (Kotas and Stasicka, 2000). Naturally occurring chromium occurs mostly in the reduced form Cr(III), which is an essential nutrient, less soluble, adsorbs strongly on solid surfaces and co-precipitates with Fe(III) hydroxides (Rai et al., 1987; Davis and Olsen, 1995). Exceptions are some rare naturally occurring Cr(VI) minerals such as the lead chromate crocoite ($PbCrO_4$) (Frost, 2004) and Cr(VI) bearing groundwater systems naturally occurring in arid regions (Izbicki et al., 2008).

Significant fractionation of the four stable Cr isotopes (^{50}Cr, ^{52}Cr, ^{53}Cr and ^{54}Cr) has been reported for a series of Cr(VI) reduction experiments (Ellis et al., 2002; Sikora et al., 2008; Berna et al., 2010; Zink et al., 2010; Dossing et al., 2011; Basu and Johnson, 2012; Han et al., 2012; Jamieson-Hanes et al., 2012; Kitchen et al., 2012). These experiments showed a general trend of accumulating heavier Cr isotopes in the unreacted Cr(VI) species and an accumulation of the lighter ones in the produced Cr(III) species. In contrast, Cr(III) species did not undergo rapid isotopic exchange during a Cr(III) oxidation experiment (Zink et al., 2010). Variation in Cr isotope composition is, therefore, an accepted proxy for demonstrating that Cr(VI) reduction is occurring in geological systems. Tracking of Cr(VI) reduction is especially powerful when dealing with subsoil Cr(VI) contamination and related remediation actions. A series of case studies demonstrating naturally occurring Cr(VI) reduction has been described recently (Izbicki et al., 2008; Berna et al., 2010; Wanner et al., 2012a,b,c). Tracking Cr(VI) reduction has also been used for unraveling redox conditions throughout Earth's history (e.g., Frei et al., 2009). In this context, observed Cr isotope fractionation was used to unravel the fluctuations in the Precambrian atmospheric oxygenation (Frei et al., 2009) and to evaluate the redox evolution of hydrothermal systems (Schoenberg et al., 2008).

Stable isotope fractionations are caused mainly by differences in the vibrational energies of isotopically light and heavy substances

* Corresponding author. Tel.: +1 5104958147; fax: +1 5104865686.
E-mail address: cwanner@lbl.gov (C. Wanner).

0009-2541/$ – see front matter © 2012 Elsevier B.V. All rights reserved.
http://dx.doi.org/10.1016/j.chemgeo.2012.11.008

Author's personal copy

(Bigeleisen and Mayer, 1947; Urey, 1947; Schauble et al., 2004). The isotopically lighter forms of any substances have a lower vibrational energy compared to the heavier ones. When substances consisting of multiple isotopic species react and the remaining reactant equilibrates with the reaction product, an unequal distribution of the isotopes is observed. Stable isotope fractionations are usually reported in terms of the isotopic fractionation factor α. For Cr isotopes, α is defined as the ratio of $^{53}Cr/^{52}Cr$ in the two stable Cr redox states (Cr(VI) and Cr(III)). For convenience, fractionation factors are often expressed as isotopic enrichment factors ε (e.g., Schauble et al., 2004; Sikora et al., 2008):

$$\varepsilon = (\alpha - 1) \cdot 1000 \approx \ln(\alpha) \cdot 1000. \quad (1)$$

Schauble et al. (2004) determined a theoretical equilibrium Cr isotope enrichment factor ε_{eq} between aqueous Cr(VI) and aqueous Cr(III) species of 6–7‰ whereas Zink et al. (2010) reported an ε_{eq} of 3.5‰ for a Cr(VI) reduction experiment conducted under highly acidic conditions (pH ≪ 1) (Table 1). In all other reported Cr(VI) reduction experiments a kinetic type isotopic fractionation behavior was observed (Ellis et al., 2002; Sikora et al., 2008; Berna et al., 2010; Zink et al., 2010; Dossing et al., 2011; Basu and Johnson, 2012; Han et al., 2012; Jamieson-Hanes et al., 2012; Kitchen et al., 2012). Applying a Rayleigh distillation model the cited Cr(VI) reduction studies determined kinetic enrichment factors ε_{kin} within the range of 0.4–5.0‰ (Table 1). Kinetic isotopic fractionation is typically observed for systems undergoing a fast net reaction where the backward reaction is negligible when compared to the overall reaction rate (Young et al., 2002; Zink et al., 2010; DePaolo, 2011).

Variations in observed effective kinetic Cr isotope enrichment factors have been attributed to several causes: (i) The reaction rate of Cr(VI) reduction affects the magnitude of the kinetic Cr isotope enrichment factor such as shown for sulfur isotope fractionation (Rees, 1973; Canfield, 2001). Sikora et al. (2008) showed a kinetic dependence on the kinetic enrichment factor for microbiologically-mediated Cr(VI) reduction experiments using lactate as the electron donor. In these experiments $\varepsilon_{kin} = 1.8$‰ was observed for a high lactate concentration and a high Cr(VI) reduction rate, and $\varepsilon_{kin} = 4.0$‰ was observed for a low lactate concentration and slow Cr(VI) reduction rate (Table 1). (ii) A variation in molecular scale reduction mechanisms has been addressed as a second cause likely inducing a variation of ε_{kin} (Sikora et al., 2008; Zink et al., 2010; Dossing et al., 2011). On the contrary, Zink et al. (2010) did not observe that the resulting Cr isotope fractionation factor is significantly dependent on the pH dependent speciation of Cr(VI) and Cr(III) species (Table 1). This is notable since the actual Cr(VI) reduction mechanism is also dependent on the pH value (e.g., pH = 7–9: $CrO_4^{2-} \Rightarrow Cr(OH)_2^+$; pH < 4: $HCrO_4^- \Rightarrow Cr^{3+}$). (iii) As a third cause, transport limitations, such as a limited diffusive flux towards reactive surfaces, have been reported to shift a system's effective ε_{kin} to lower values (Bender, 1990; Brandes and Devol, 1997; Green et al., 2010). Even though these studies described other isotopic systems (NO_3^-- and O_2-reduction) it is assumed that transport limitations can also affect the kinetic Cr isotopic enrichment factor (Berna et al., 2010).

To the author's knowledge no study has yet quantitatively assessed the individual contributions of the reaction mechanism, the Cr(VI) reduction rate, and transport limitations on the effective kinetic Cr isotope enrichment factor. In this study these contributions were quantitatively addressed by performing a series of reactive transport model simulations of Cr(VI) reduction in a porous medium along a 1D flow path. In the second part, the Fe(II)-added–Cr(VI) reduction experiments performed by Dossing et al. (2011) were simulated and an alternative interpretation proposed.

2. Simulation of Cr(VI) reduction in porous media along a 1D flow path

2.1. Conceptual model

As a model simplification, it is assumed that Cr(VI) reduction occurs at solid surfaces only (Fig. 1). This assumption is based on the observation that Fe(II)-bearing minerals and solid organic matter are the most common naturally occurring Cr(VI) reducing agents (Palmer and Puls, 1994). For both cases, Cr(VI) reduction can be microbiologically-mediated if specific microorganisms are present (Sikora et al., 2008; Han et al., 2010). Most bacteria are fixed on solid surfaces and are

Table 1
Summary of published Cr(VI) reduction experiments.

Reference	e^--Donor	Initial Cr(VI)	Fractionation mode	Effective ε	Comment
Ellis et al. (2002)	Fe^{2+} bearing minerals (magnetite)	0.19 μM/L	Rayleigh-type	3.3 and 3.5‰	
Schauble et al. (2004)	Theoretical calculation		Equilibrium fractionation	6–7‰	
Sikora et al. (2008)	3.3–100 mM lactate	5.1–9.5 μM	Rayleigh-type	4.1–4.5‰	Bioreduction (*Shewanella oneidensis*). Rate = $42 \cdot 10^{-18}$ mol/cell/day[a]
	10,200 mM lactate	9.5 μM	Rayleigh-type	1.8‰	Bioreduction (*Shewanella oneidensis*). Rate = $450 \cdot 10^{-18}$ mol/cell/day[a]
Zink et al. (2010)	0.9 μM H_2O_2	0.9 μM	Rayleigh-type[b]	4.2‰	pH = 0.7
	0.9 μM H_2O_2	0.9 μM	Equilibrium fractionation[b]	7.2‰	pH = 0.7
	13.2 μM H_2O_3	0.9 μM	Rayleigh-type	5.0‰	pH = ca. 7
	13.2 μM H_2O_4	0.9 μM	Equilibrium fractionation	3.5‰	pH ≪ 1
Berna et al. (2010)	Fe^{2+} bearing minerals (e.g. green rust)	1.92 μM	Rayleigh-type	2.4 and 3.1‰	
Dossing et al. (2011)	0.05 nM Fe^{2+} (batch experiment)	0.42 nM	Rayleigh-type	3.1–4.5‰	
	0.03 mM Fe^{2+}/min (added experiment)	0.78 μM	Rayleigh-type	1.5‰	
Han et al. (2012)	20 mM lactate	50 μM	Rayleigh-type	2‰	Bioreduction (*Pseudomonas stutzeri*); aerobic conditions
	20 mM lactate	50 μM	Rayleigh-type	0.4‰	Bioreduction (Pseudomonas Stutzeri); denitrifying conditions
Basu and Johnson (2012)	Fe(II) doped goethite	17.7 μM	Rayleigh-type	3.91‰	
	FeS (75 μM Fe(II))	19 μM	Rayleigh-type	2.11‰	
	Green rust (100 μM Fe(II))	11 μM	Rayleigh-type	2.65‰	
	$FeCO_3$ (84.2 μM Fe(II))	19 μM	Rayleigh-type	2.67‰	
	4 g of reduced sediment	24 μM	Rayleigh-type	3.18‰	
Kitchen et al. (2012)	60 mM Fe^{2+}	20–22 μM	Rayleigh-type	4.20 ± 0.11‰	pH = 4–5.3
	10 mg humic and 200 μM fulmic acid	21 μM	Rayleigh-type	3.11 ± 0.11‰	pH = 4.5–5
Jamieson-Hanes et al. (2012)	7.5 g organic C (batch experiment)	100 μM	Rayleigh-type	3.50 ± 0.1‰	

[a] Rate observed during first 24 h of experiment.
[b] Fractionation mode not clear since all experiment resulted in the same extent of Cr(VI) reduction. Presented here are the two different possibilities for interpretation (equilibrium vs. kinetic fractionation).

Author's personal copy

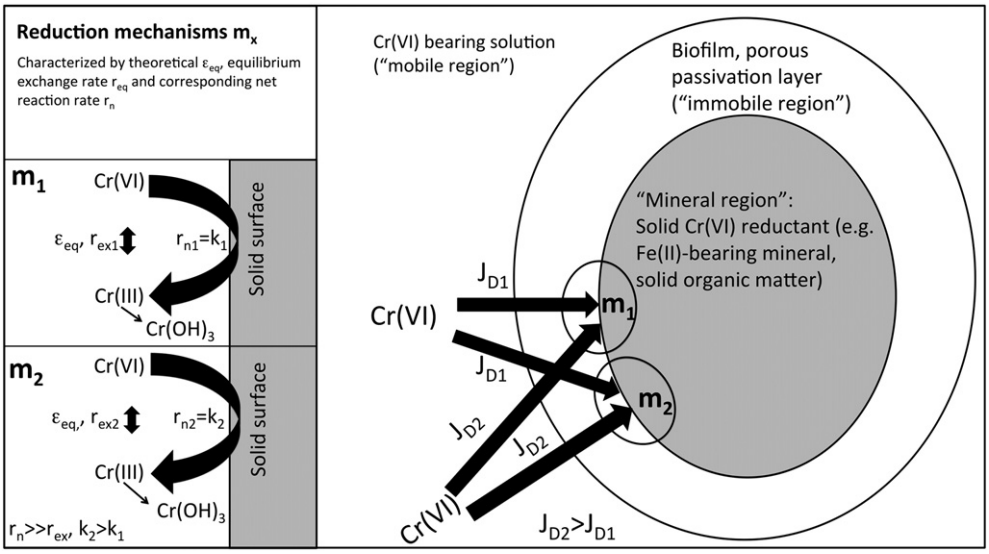

Fig. 1. Conceptual model used to simulate Cr isotope fractionation for porous media along a 1D flow path. The model assumes that Cr(VI) reduction to Cr(III) occurs at solid surfaces and that Cr(III) immediately precipitates as $Cr(OH)_3$ (see inset). Overall Cr(VI) reduction rate is a function of diffusive Cr(VI) transport (J_D) to the solid surface and the net reduction rate r_n. Cr isotope fractionation typically occurs in the surface reaction controlled regime, where r_n is much larger than the gross exchange rate r_{ex} (DePaolo, 2011). The model allows simulating the magnitude of Cr isotope fractionation as a function of different diffusive Cr(VI) fluxes (e.g., J_{D1} and J_{D2}) for one specific reduction mechanisms (characterized by ε_{eq}) occurring at different net molecular reaction rates (e.g., r_{n1} and r_{n2}). For the specified reaction network the reaction rate constant k (Eqs. (6) and (7)) represents a proxy for r_n. The terms "mineral region", "immobile region", and "mobile region" refer to the multi-region approach (Xu, 2008) that was used to setup the model.

immobile (Harvey et al., 1989). Moreover, Cr(VI) reaction products (e.g., $Cr(OH)_3$) passivate the reactive surface sites of solid Cr(VI) reducing agents (Jeen et al., 2007). Accordingly, a passivation layer and/or biofilm is formed around solid surfaces and Cr(VI) has to diffuse through such layers in order to get reduced.

The proposed conceptual model is closely related to the surface kinetic model recently described by DePaolo (2011) to explain Ca isotope fractionation during calcite precipitation experiments. According to DePaolo (2011) surface reactions can occur in four different regimes: (i) a near equilibrium regime, where the net reaction rate (r_n) is much slower than the forward and backward reaction rates (e.g., exchange rate r_{ex}, Fig. 1), respectively, (ii) a surface equilibrium regime with the same requirements than in the near equilibrium regime but with a r_n that is fast enough to induce transport limitations, (iii) a surface reaction limited regime where $r_n \gg r_{ex}$ and (iv) a regime with transport and reaction effects where $r_n \gg r_{ex}$ and with a transport limitation of r_n.

Cr(III), which is the reaction product of Cr(VI) reduction, is almost insoluble over a wide pH-range (Rai et al., 1987) and it is assumed that it almost instantaneously precipitates as $Cr(OH)_3$. Consequently, Cr(VI) reduction either occurs in a surface reaction limited regime, with or without transport limitations induced by the diffusive transport of Cr(VI) through the biofilm, and/or passivation layer (Fig. 1). According to the model of DePaolo (2011), both regimes should tend to enrich the light (e.g., Cr) isotope in the reduced phase (Cr(III)) and a kinetic-type Cr isotope fractionation would be observed.

Our conceptual model (Fig. 1) allows the individual assessment of kinetic Cr isotope fractionation effects induced by surface reaction kinetics and by transport limitation effects, respectively. It assumes that Cr(VI) reduction occurs as one single molecular-scale Cr(VI) reduction mechanism, which is described by a specific equilibrium enrichment factor (Urey, 1947). Accordingly, one single equilibrium enrichment factor ε_{eq} was defined, representing a hypothetical near-equilibrium regime (DePaolo, 2011). Kinetic effects on the effective Cr isotope enrichment factor were assessed by a variation of the specific molecular scale Cr(VI) reduction rate (k) at a constant, non-transport-limited diffusive Cr(VI) flux J_D through the biofilm and/or surface passivation layer (Fig. 1). In contrast, transport limitations were assessed by varying J_D at a constant molecular scale Cr(VI) reduction rate k. Each Cr isotopic species ($^{52}CrO_4^{2-}$ and $^{53}CrO_4^{2-}$) were treated as separate transported species as done for ^{18}O and ^{16}O in Singleton et al. (2004). Fractionation effects due to a variation in diffusion coefficient between ^{52}Cr and ^{53}Cr species were not considered. If the diffusion coefficients differed, our model approach would induce Cr isotope fractionation also due to variation in the diffusive flux within the biofilm and/or passivation layer such as described for Sr isotopes (Watson and Mueller, 2009). This model simplification is justified by the fact that mass differences between the different isotopic Cr(VI) species are rather small (115 vs. 116 g/mol for CrO_4^{2-}).

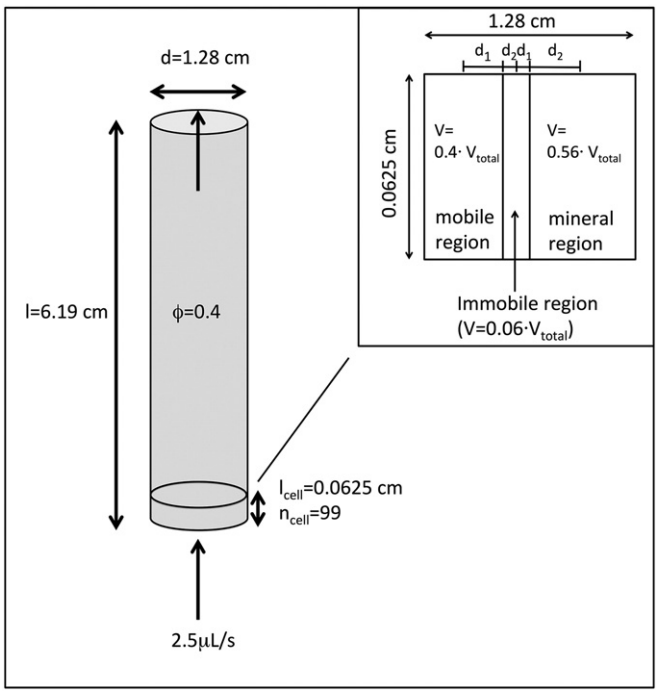

Fig. 2. General setup used to model Cr(VI) reduction along a 1D flow path. The inset gives the front view of one individual grid cell and illustrates how the 99 cells were discretized into the three regions of our multi-region approach.

Author's personal copy

Table 2
Composition of the injecting fluid.

pH		8.06
$^{53}CrO_4^{2-}$	mol/L	5.09E−07[a]
$^{52}CrO_4^{2-}$	mol/L	4.49E−06[a]
K^+	mol/L	1.46E−03
HCO_3^-	mol/L	1.90E−03
SO_4^{2-}	mol/L	8.06E−05
Ca^{2+}	mol/L	2.28E−04
Fe^{2+}	mol/L	1.00E−04

[a] $\delta^{53}Cr = 0.0‰$.

Table 4
Thermodynamic properties of specified mineral reactions.

Reaction	log K (equilibrium constant)[a]
$^{52}CrO_4^{2-} + 5H^+ + 3Fe^{2+} = {}^{52}Cr(OH)_{3(s)} + 3Fe^{3+} + H_2O$	25.69147912
$^{53}CrO_4^{2-} + 5H^+ + 3Fe^{2+} = {}^{53}Cr(OH)_{3(s)} + 3Fe^{3+} + H_2O$	25.69
$CaCO_3 + H + = Ca^{2+} + HCO_3^-$	1.8487
$Fe^{3+} + 3H_2O = Fe(OH)_3 + 3H^+$	−3.191

[a] At 25 °C.

2.2. Model setup

Cr isotope fractionation effects were simulated for a porous media along an approximately 6.2 cm long 1D flow path (Fig. 2). This model domain was divided into 99 cylindrical cells, each having a thickness of 0.0625 cm. An injection rate of 2.5 μL/s was specified for the first cell and the overall porosity was set to 0.4. These specifications lead to an average linear flow velocity of 7 cm/day simulating Cr(VI) transport that is dominated by advection such as reported for a series of field site Cr(VI) contaminations (Faybishenko et al., 2008; Flury et al., 2009; Wanner et al., 2012a,b,c). The composition of the injecting fluid was specified as listed in Table 2.

The multi-region model approach described by Xu (2008) was used to numerically formulate the conceptual model (Fig. 1). In doing so, a three region model was defined and each of the 99 cells along the column were divided into these three regions (Fig. 2): (i) a mobile region where advective transport occurs, (ii) an immobile region that is affected by diffusive transport only and (iii) a mineral region where mineral dissolution/precipitation reactions take place (Figs. 1 and 2).

Table 3 gives the physical and mineralogical parameters used for the three regions. Porosity and permeability were defined in a similar way as Xu (2008). The distance between the regions and the corresponding interfacial areas were calculated according to the general geometrical setup of the simulated column (Fig. 2).

Transport processes were modeled according to the standard advection diffusion equation in TOUGHREACT (Xu et al., 2011)

$$\frac{\partial(\phi C_i)}{\partial t} = \nabla\cdot(\phi\cdot D_i\cdot\tau\cdot\nabla C_i) - \nabla\cdot(\phi\cdot v\cdot C_i) \quad (2)$$

where C_i (mol/kg$_{H2O}$) refers to the concentration of aqueous species i, ϕ is the porosity of the porous medium, D_i (m^2/s) refers to the diffusion coefficient of species i, τ refers to the tortuosity, and v (m/s) is the average linear flow velocity. Advective transport takes place essentially only within the mobile region because the permeability of this region is much higher when compared to the other regions (Table 3). Diffusive flux of aqueous species i (J_{Di}) within the immobile region is proportional to

$$J_{Di} \propto \frac{D_{aq}\cdot A}{d_1 + d_2} + \frac{dC_i}{dx} \quad (3)$$

where D_{aq} refers to the diffusion coefficient of aqueous species (~10^{-9} m^2/s), A (m^2) is the interfacial area between two adjacent regions, dC_i/dx (mol/kg$_{H_2O}$/m) is the concentration gradient of species i, and d_1 and d_2 (m) refer to the distances from the centers of two adjacent regions to their mutual interface (Fig. 2).

2.3. Reaction network

Ferrous iron was used as a general Cr(VI) reducing agent. This choice is based on the observation that ferrous iron is one of the most prevalent naturally occurring Cr(VI) reducing agents (Buerge and Hug, 1997). Furthermore, it was assumed that once produced, Cr(III) immediately precipitates as $Cr(OH)_3$. This simplification is justified by the fact that the simulations were performed for systems at near neutral pH-values where the solubility of $Cr(OH)_3$ is low and $Cr(OH)_{3(aq)}$ is the dominant Cr(III) species (Rai et al., 1987; Kotas and Stasicka, 2000). Following this argument, Cr(VI) reduction to Cr(III) was formulated for two Cr isotope species (^{52}Cr and ^{53}Cr) as a kinetic mineral precipitation reaction using Fe(II) as reducing agent:

$$^{52}CrO_4^{2-} + 5H^+ + 3Fe^{2+} = {}^{52}Cr(OH)_{3(s)} + 3Fe^{3+} + H_2O \quad (4)$$

$$^{53}CrO_4^{2-} + 5H^+ + 3Fe^{2+} = {}^{53}Cr(OH)_{3(s)} + 3Fe^{3+} + H_2O \quad (5)$$

It should be pointed out that the coexistence of aqueous Fe(II) and Cr(VI) such as defined for the injecting fluid (Table 2) is not favored from a thermodynamic point of view (Table 4) because the homogenous reaction between Fe^{2+} and CrO_4^{2-} is nearly instantaneous (Buerge and Hug, 1997). Moreover, the simulations were run for circumneutral pH values at which Fe(II) species are only stable if strongly reducing conditions are established (Nordstrom and Munoz, 1985). Although these initial conditions are in disequilibrium, the specified reaction network allows simulation of Cr(VI) reduction at solid surfaces. This was achieved by allowing $Cr(OH)_3$ precipitation and Cr(VI) reduction under kinetic constraints (Eqs. (4) and (5)) within the mineral region only (Fig. 1) while the homogenous reaction between Fe^{2+} and CrO_4^{2-} is suppressed in the other regions. With these specifications, aqueous Fe(II) operates as a representative for any solid or immobile Cr(VI) reducing agents (e.g., bacteria, Fe(II)-bearing minerals), and not as an aqueous reducing agent. Accordingly, the reaction network is in agreement with our

Table 3
Physical and mineralogical parameters of the three regions of the specified multi-region model.

Parameter	Mobile region		Immobile region		Mineral region	
Volume fraction of the medium	0.4		0.06		0.54	
Porosity	1		1		0.05	
Distance to interface (m)	d_1	d_2	d_1	d_2	d_1	d_2
		2.27E−03	3.40E−04	3.40E−04	3.06E−03	
Area between regions (m^2)		1.09E−02		1.09E−02		
Permeability (m^2)	1.00E−11		1.00E−18		1.00E−18	
Mineralogy	No mineral reaction allowed		No mineral reaction allowed		10 vol.% Calcite, $Fe(OH)_3$ and $Cr(OH)_3$ precipitation (Cr(VI) reduction) allowed, remaining solids are non-reactive	

Author's personal copy

conceptual model assuming that Cr(VI) reduction occurs at solid surfaces only (Fig. 1). The benefit of using aqueous Fe(II) as a representative for Fe(II)-bearing solids is that molecular scale heterogeneous Cr(VI) reduction at reactive Fe(II) surfaces do not have to be formulated explicitly. The same holds true for iron cycling phenomena, such as the partial reductive dissolution of Fe(III)-bearing solids, subsequent homogeneous reactions between aqueous Fe(II) with Cr(VI) and reprecipitation of Fe(III)-bearing solids (Coby et al., 2011). The definition of excess aqueous Fe(II) with respect to Cr(VI) in the injecting fluid (Table 2) ensures that Fe(II) consumption caused by Cr(VI) reduction (Eqs. (4) and (5)) does not affect the overall Cr(VI) reduction rate. In addition, this definition allows specifying constant iron-reducing redox conditions along the entire 1D flow path.

The isotopic endmembers $^{52}Cr(OH)_{3(s)}$ and $^{53}Cr(OH)_{3(s)}$ were treated as one mineral phase assuming an ideal solid solution. In doing so, TOUGHREACT (Xu et al., 2011) calculates the reaction rates of the $^{52}Cr(OH)_3$ ($r^{52}{}_{Cr}$) and $^{53}Cr(OH)_3$ ($r^{53}{}_{Cr}$) endmembers according to Eqs. (6) and (7),

$$r_{^{52}Cr} = A_{ss} \cdot k_{52} \cdot \left(1 - \frac{Q_{^{52}Cr}}{K_{^{52}Cr} X_{^{52}Cr}}\right) = A_{ss} \cdot k \cdot \left(1 - \frac{Q_{^{52}Cr}}{K_{^{52}Cr} X_{^{52}Cr}}\right) \quad (6)$$

$$r_{^{53}Cr} = A_{ss} \cdot k_{53} \cdot \left(1 - \frac{Q_{^{53}Cr}}{K_{^{53}Cr} X_{^{53}Cr}}\right) = A_{ss} \cdot k \cdot \left(1 - \frac{Q_{^{53}Cr}}{K_{^{53}Cr} X_{^{53}Cr}}\right) \quad (7)$$

where A_{ss} refers to the reactive surface area of the solid solution ($m^2{}_{mineral}/kg_{H_2O}$), k_{52} and k_{53} are the reaction rate constants of the two end members (mol/m^2/s), $Q^{52}{}_{Cr}$ and $Q^{53}{}_{Cr}$ refer to the ion activity product of the Cr(VI) reduction reaction (Eqs. 4 and 5), $K^{52}{}_{Cr}$ and $K^{53}{}_{Cr}$ are the corresponding equilibrium constants and X_{52} and X_{53} are the mole fractions of the two end members. k_{52} and k_{53} represent the kinetics of the actual molecular scale Cr(VI) reduction reaction. As a model simplification, k_{52} and k_{53} were assumed to be equal and they were treated as one variable k (Eqs. (6) and (7)). This model simplification holds perfectly true for an equilibrium situation where the net Cr(VI) reduction rate is zero but also for an infinitely high net overall Cr(VI) reduction rate, where Cr(VI) is reduced to Cr(III) instantaneously. The total reactive surface area of the $Cr(OH)_3$ solid solution, A_{ss}, was held constant and was fixed to an arbitrary value of 0.014 m^2/kg_{H_2O}. Assuming an initial $Cr(OH)_3$ volume fraction of 10^{-6}, this value corresponds to a specific surface area of 600 m^2/g that is typically used for ferric hydroxides (Dzombak and Morel, 1990). The assumption of constant surface area is based on the fact that the overall Cr(VI) reduction rate is not dependent on the reactive surface area of the $Cr(OH)_3$ solid solution because $Cr(OH)_3$ is not a Cr(VI) reducing agent. However, the rate is dependent on the reactive surface area of solids operating as Cr(VI) reducing agents. To keep things simple, evolving reactive surface areas of solid Cr(VI) reducing agents were not considered by our reaction network. In doing so, our reaction network does not account for the fact that solid Cr(VI) and Fe(II) bearing reductants get passivated by newly-formed reaction products such as $Cr(OH)_{3(s)}$, $Fe(OH)_3$ and carbonates, that may reduce the reactive surface areas with time (Jeen et al., 2007; Wanner et al., 2011). The cited studies also provide two alternative reaction networks that allow simulating the gradual decline of the reactive surface area. These reaction schemes, however, were not included, since reactions with Fe(II) bearing solids were not formulated explicitly and the focus of this work was not on the long term reactivity of solid Cr(VI) reducing agents. The ideal behavior of the $Cr(OH)_3$ solid solution was ensured by Eq. (8) (e.g., Reed, 1982)

$$\frac{Q_{ss}}{K_{ss}} = \left(\frac{Q_{^{52}Cr}}{K_{^{52}Cr}}\right) + \left(\frac{Q_{^{53}Cr}}{K_{^{53}Cr}}\right) \quad (8)$$

while a rate law derived from transition state theory (TST) (Lasaga, 1984) was applied for the solid solution using Eq. (9)

$$r_{ss} = A_{ss} \cdot k \cdot \left(1 - \frac{Q_{ss}}{K_{ss}}\right). \quad (9)$$

In these equations, Q_{ss} and K_{ss} refer to the ion activity product and the equilibrium constant of the solid solution, r_{ss} and k are the overall solid solution's reaction rate and reaction rate constant and A_{52} and A_{53} refer to the reactive surface area of the two end members.

Using the solid solution approach described above, Cr isotope fractionation is simulated by means of varying equilibrium constants $K^{52}{}_{Cr}$ and $K^{53}{}_{Cr}$ only. According to Urey (1947) $K^{52}{}_{Cr}/K^{53}{}_{Cr}$ refers to the theoretical equilibrium fractionation factor α_{eq} for one specific Cr(VI) reduction mechanism. A log(K) of 25.69 was taken for Eq. (5) (Table 4). This value was calculated based on Fe speciation reactions and log(K) values tabulated in the EQ3/6 database (Wolery, 1992) which was derived using SUPCRT92 (Johnson et al., 1992 and references therein) and on thermodynamic Cr data reported by Ball and Nordstrom (1998). The log(K) of Eq. (4) was then set at 25.69147912 (Table 4) to express an equilibrium Cr enrichment factor ε_{eq} of 3.4‰ (i.e., corresponding to $\alpha_{eq} = 10^{25.69147912}/10^{25.69} = 1.0034$). This value approximately represents the average of experimentally determined kinetic Cr isotope enrichment factors (Table 1) and is close to the equilibrium Cr isotope enrichment factor of 3.5‰ that was determined by Zink et al. (2010).

Isotopic data are reported as the $^{53}Cr/^{52}Cr$ ratio in terms of the δ-notation relative to the certified Cr isotope standard NIST SRM 979 and are given in ‰:

$$\delta^{53}Cr = \left(\frac{\left(^{53}Cr/^{52}Cr\right)_{modeled}}{\left(^{53}Cr/^{52}Cr\right)_{SRM979}}\right) - 1 \quad (10)$$

$(^{53}Cr/^{52}Cr)_{modeled}$ is the simulated $^{53}Cr/^{52}Cr$ ratio and $(^{53}Cr/^{52}Cr)_{SRM979}$ the known $^{53}Cr/^{52}Cr$ ratio (=0.11339) of the certified standard.

In addition to $Cr(OH)_3$ precipitation, the reaction network allows the formation of $Fe(OH)_3$ also:

$$Fe^{3+} + 3H_2O = Fe(OH)_3 + 3H^+. \quad (11)$$

Additionally, 10 vol.% of calcite (Table 4) was added to buffer pH changes induced by Cr(VI) reduction (Eqs. (4) and (5)). $Fe(OH)_3$ and calcite precipitation and dissolution reactions were simulated using a thermodynamic approach. Hence, they were allowed to reach thermodynamic equilibrium at each time step. Equilibrium constants for mineral and aqueous species reactions were defined as tabulated in the EQ3/6 database (Wolery, 1992) (Table 4).

2.4. Model results and discussion

The model was run for four different overall Cr(VI) reduction rates by means of a varying Cr(VI) reduction reaction rate constant k (Eqs. (6) and (7)), keeping ε_{eq} constant at 3.4‰. Following the discussion by DePaolo (2011), these runs assessed Cr isotope fractionation in reaction rate controlled regimes as a function of the actual surface reaction rate k (Fig. 1). In a second set of another four model runs, Cr isotope fractionation effects in transport-controlled regimes (DePaolo, 2011) were simulated. For these simulations, the system's overall Cr(VI) reduction rate was varied by means of a varying diffusive flux J_D within the immobile region (Fig. 1) while keeping k constant ($k/k_{max} = 0.1$). The interfacial area A between the three regions was varied by ca. 2.2 orders of magnitude resulting in a variation of the diffusive flux J_D in the same order of magnitude (Eq. (3)). The use of a set of different diffusive fluxes J_D operates as a proxy for a variation in the

Author's personal copy

extent of the biofilm/passivation layer present around reactive surfaces (Fig. 1). This approach also allows considering the assumption that a biofilm/biological reaction system may have different effective J_D than an equivalently thick chemical passivation layer, which is based on the observation that the permeability of biological reaction systems (e.g., cell membranes) can be relatively low (Hancock and Wong, 1984; Pearson et al., 1999; Nikaido, 2003; Jones and Niederweis, 2010). Small values for J_D correspond to a thick passivation layer or a slow transport path within biological systems. On the contrary, large J_D corresponds to a thin passivation layer or fast transport paths of biological systems. According to DePaolo (2011), transport limitations of chemical systems are a function of the thickness of such layers and occur only when it is larger than a specific minimum extent. Moreover, the thickness highly depends on a specific experimental setup. In a stirred batch experiment for instance, the passivation layer is much smaller when compared to an unstirred experiment. Accordingly, the definition of different values for J_D allows assessing the contribution of transport limitations induced by a specific experimental setup or by specific passivation phenomena on the effective kinetic Cr isotope enrichment factor.

Modeled steady-state Cr(VI) concentration profiles within the mobile region followed a linear trend in a logarithmic C/C_0 plot, where C and C_0 refer to the Cr(VI) concentration at a specific location and at the column inlet (Figs. 3a and 4a). Accordingly, Cr(VI) reduction within the model domain was simulated by means of a first order rate law with respect to the Cr(VI) concentration. We are confident that this is a reasonable simulation of natural systems since a first order behavior has been reported for experiments performed at fixed pH values and in

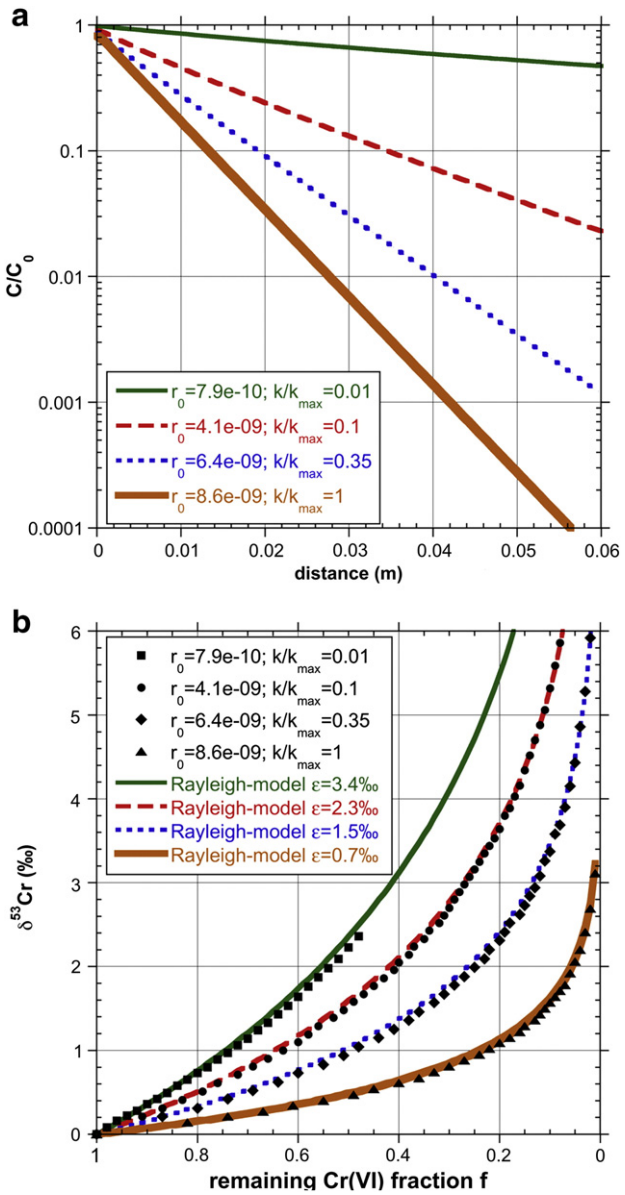

Fig. 3. Model results for varying overall Cr(VI) reduction rates (r_0 = reaction rate in mol/kg$_{H_2O}$/s at column inlet) defined by means of differing molecular scale Cr(VI) reduction rates k (surface reaction controlled regime) using a constant equilibrium enrichment factor of 3.4‰. a: Steady state Cr(VI) concentration profiles (C/C_0) within the mobile region. b: δ^{53}Cr vs. reduced Cr(VI) fraction plots for aqueous Cr(VI) of the mobile region. Also shown is the theoretical δ^{53}Cr evolution of mobile region Cr(VI) following a Rayleigh-type model for ε_{kin} = 3.4‰, 2.3‰, 1.5‰ and 0.7‰.

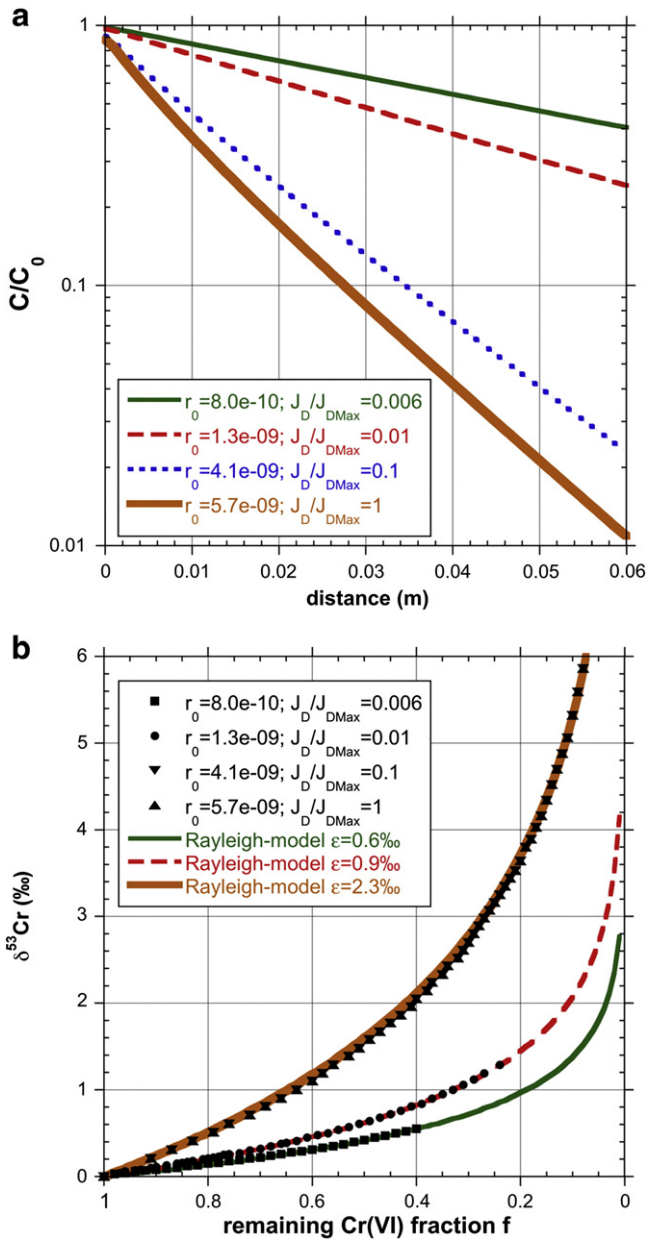

Fig. 4. Model results for varying overall Cr(VI) reduction rates (r_0 = reaction rate in mol/kg$_{H_2O}$/s at column inlet) defined by means of varying diffusive fluxes J_D within the immobile region (transport-limited regime). a: Steady state Cr(VI) concentration profiles (C/C_0) within mobile region. b: δ^{53}Cr vs. reduced Cr(VI) fraction plots for aqueous Cr(VI) of the mobile region. Also shown is the theoretical δ^{53}Cr-evolution of mobile region Cr(VI) following a Rayleigh-type model for ε_{kin} = 2.3‰, 0.9‰ and 0.6‰.

Author's personal copy

the presence of an excess of Cr(VI) reducing agents (Buerge and Hug, 1997). δ^{53}Cr vs. remaining Cr(VI) fraction plots that correspond to the Cr(VI) concentration profiles are illustrated in Figs. 3b and 4b. Modeled δ^{53}Cr-values fit closely with Rayleigh-type fractionation curves expressed as

$$\delta^{53}Cr_x = ((\delta^{53}Cr_0 + 1000)f^{(\alpha kin-1)}) - 1000 \quad (12)$$

where $\delta^{53}Cr_x$ and $\delta^{53}Cr_0$ refer to the Cr isotope composition at location x and at the column inlet (0.0‰, see Table 2), f refers to the remaining Cr(VI) fraction at location x and αkin is the effective kinetic fractionation factor.

Depending on the regime, ε_{kin} showed a different dependence on the overall Cr(VI) reduction rate. For the surface reaction controlled regimes ε_{kin} decreased with increasing overall Cr(VI) reduction rate even though the equilibrium enrichment factor and reduction mechanism, respectively, remained the same (Fig. 3b). These model runs also show that ε_{kin} approaches the defined equilibrium enrichment factor (ε_{eq} = 3.4‰) at slow overall Cr(VI) reduction rates (Fig. 3b). This observation indicates that the maximum effective Cr isotope enrichment factor is defined by the (theoretical) equilibrium enrichment factor for a given Cr(VI) reduction mechanism.

In contrast, ε_{kin} became smaller with decreasing overall Cr(VI) reduction rate for the transport-limited regimes (Fig. 4b). Interestingly, ε_{kin} approaches a maximum value of 2.3‰ for the condition where a high diffusive flux within the immobile region was specified (J_D/J_{Dmax} = 0.1 and J_D/J_{Dmax} = 1, Fig. 4b). This observation confirms that for non-transport-limited systems, the resulting Cr isotope enrichment factor solely depends on the equilibrium enrichment factor and on the molecular scale Cr(VI) reduction rate.

Regarding the interpretation of experimentally determined kinetic Cr isotope enrichment factors, an important observation is that ε_{kin} does not a priori depend on a system's overall Cr(VI) reduction rate. Such dependence is only true for systems that do not encounter transport limitations. Furthermore it has to be noticed that both high molecular scale Cr(VI) reduction rates and transport limitations can significantly shift the observed ε_{kin} to low values even though the specific Cr(VI) reduction mechanism remains constant.

The observation that simulated δ^{53}Cr-values followed a Rayleigh-type fractionation model lends support that such Rayleigh models are a suitable approach to describe Cr isotope fractionation in dynamic systems and not for well-controlled laboratory experiments only. For example, Fig. 5 illustrates for one particular model run that δ^{53}Cr-values of $Cr(OH)_3$ present within the mineral region can also be approximated with a Rayleigh-type model. It has to be pointed out that the Rayleigh behavior of solid Cr(III) was calculated by means of the same equation as for the Cr(VI) present within the mobile region (Eq. (12)). In contrast, δ^{53}Cr-values of solids obtained from closed system batch experiments follow the Rayleigh curve "Cr(III) Rayleigh-model (accumulation)" (Fig. 5), which accounts for the fact that all solids present within the system accumulate over time (Zink et al., 2010). Accordingly, it is suggested that δ^{53}Cr-values collected during flow-through experiments or at field sites follow the non-accumulative-Rayleigh curve such as proposed by Wanner et al. (2012a). The accuracy of such Rayleigh-models do, however, suffer from uncertainties in the magnitude of the effective field scale kinetic Cr isotope enrichment factor.

3. Model application: simulation of the Dossing et al. (2011) Fe(II)–Cr(VI) reduction experiment

After having shown that variations in kinetic Cr isotope enrichment factors are not necessarily due to changes in Cr(VI) reduction mechanisms, an alternative interpretation is proposed for the Dossing et al. (2011) Fe(II)-added–Cr(VI) reduction experiment. This new interpretation is tested with another reactive transport model.

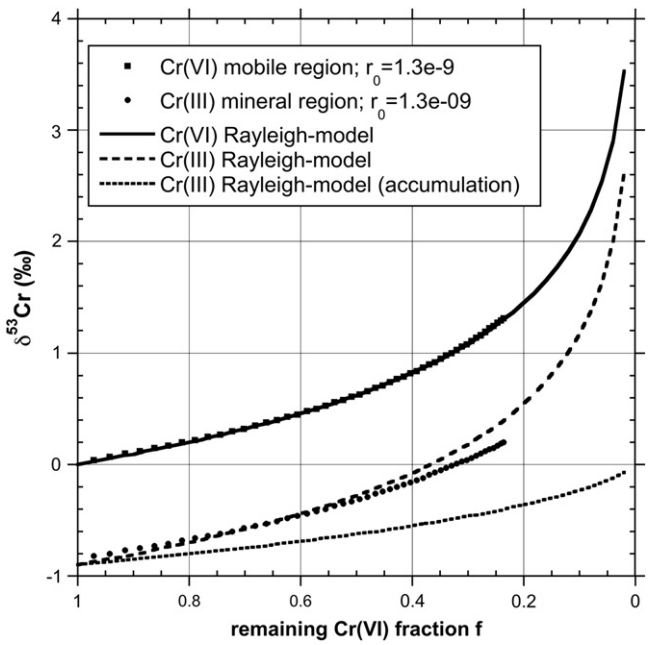

Fig. 5. Rayleigh model for one model run simulating a transport-limited regime (J_D/J_{Dmax} = 0.01). δ^{53}Cr-values of Cr(VI) within the mobile region and δ^{53}Cr-values of Cr(III) within the mineral region follow a Rayleigh fractionation model with ε_{kin} = 0.9‰. Also shown is the theoretical δ^{53}Cr evolution of total Cr(III) produced along the 1D flow path (curve 'Cr(III) accumulation').

The experiment was performed by adding a ferrous iron solution at a constant flow rate into a beaker containing a Cr(VI) bearing solution (Dossing et al., 2011). During the course of the experiment the pH-value was fixed to 8.1. The initial Cr(VI) bearing solution was completely reduced within a time period of ca. 70 min. δ^{53}Cr-values of precipitated solid Cr(III) revealed a kinetic Cr isotope enrichment factor of 1.5‰ (Table 1). In contrast, a kinetic enrichment factor of 3.1–4.5‰ was observed for a batch experiment with a fixed initial CrO_4^{2-} and Fe^{2+} concentration (Table 1). Dossing et al. (2011) attributed the low enrichment factor observed in the iron-added experiment to a Cr(VI) reduction mechanism involving the formation of green rust, adsorption of CrO_4^{2-} anions and Cr(VI) reduction within the green rust structure. Alternatively, a kinetic cause for the low observed enrichment factor was ruled out explicitly since it was argued that the Cr(VI) reduction rate was lower in the iron-added experiment when compared to the batch experiment. This statement, however, represented only a qualitative interpretation since actual molecular scale Cr(VI) reduction rates were not quantified explicitly. It is based on the fact that for the Fe(II)-added experiment Fe(II) was added slower than in the batch-experiment where it was injected instantaneously (see Dossing et al., 2011 for more details).

3.1. Conceptual model

In this model we test the assumption of Dossing et al. (2011) that the Cr(VI) reduction rate was low in the iron-added experiment. To test this assumption, a different conceptual model was used to constrain the reactive transport model (Fig. 6). It is known that in the presence of aqueous Fe(II) and at near neutral pH values or at acidic conditions (pH<3), Cr(VI) is reduced to Cr(III) at a very high reaction rate that is proportional to the Fe(II)/Cr(VI) ratio (Buerge and Hug, 1997). We assume that the Fe(II)/Cr(VI) ratio and the Cr(VI) reduction rate in the vicinity of the Fe(II) inlet location were higher than in the batch experiment. This assumption is based on the observation that the overall $Fe(II)_{added}/Cr(VI)_{initial}$ ratio of the iron-added experiment was the same as the initial Fe(II)/Cr(VI) ratio of the batch experiment after only ca. 3 min (Dossing et al., 2011). Consequently, it is

Author's personal copy

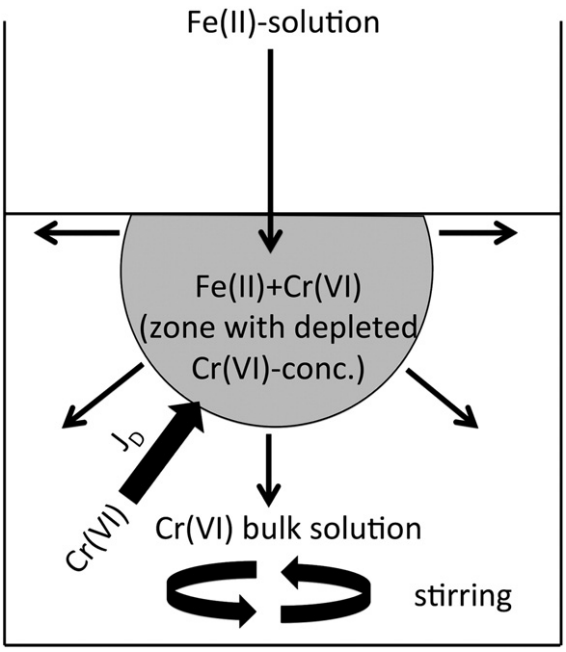

Fig. 6. Conceptual model for simulating the Fe(II)-added–Cr(VI) reduction experiment performed by Dossing et al. (2011): Cr(VI) reduction occurs at a high reaction rate but only within a limited volume with a sufficient amount of Fe(II) (gray domain). Cr(VI) exchange between bulk solution and depletion zone occurs via stirring and diffusive Cr(VI) flux J_D. During the course of the experiment this Cr(VI)-depleted domain increases due to a decrease in the overall Cr(VI) concentration and a wider spread of injected Fe(II).

proposed that a zone with a depleted Cr(VI) concentration and complete Fe(II) consumption was established at the inlet location (Fig. 6). Moreover, it is assumed that the pH-value of the depletion zone is locally different when compared to the bulk solution since Cr(VI) reduction and subsequent $Fe(OH)_3$ precipitation lead to a significant pH change (Eqs. (4), (5) and (11)).

Cr(VI) exchange between the bulk solution and the depletion zone occurred via stirring but also due to a diffusive flux induced by the proposed Cr(VI) concentration gradient (Eq. (3)). The diffusive Cr(VI) flux J_D (Eq. (3)) towards the depletion zone was likely decreasing during the course of the experiment since the bulk Cr(VI) concentration and Cr(VI) concentration gradient, respectively, were decreasing with time (Dossing et al., 2011). The decrease in diffusive Cr(VI) flux most likely led to a gradual increase of the volume of the proposed Cr(VI) depletion (and Fe(II) consumption) zone until it covered the whole experimental volume. This stage corresponds to the time in the experiment when the bulk Cr(VI) concentration was below the detection limit and the Fe(II) concentration started to increase (Dossing et al., 2011).

Because the proposed conceptual model assumes a high molecular scale Cr(VI) reduction rate, which is possibly transport-limited, Cr isotope fractionation is expected to encounter surface reaction as well as transport effects (DePaolo, 2011). These are the requirements where ε_{kin} is most effectively shifted to low values as shown with the simulations presented earlier (Figs. 3 and 4).

3.2. Model setup and simulation results

The same reaction network as described earlier was used to simulate Cr(VI) reaction and Cr isotope fractionation, assuming that Cr(VI) reduction occurs as a single molecular-scale reaction mechanism with a hypothetical equilibrium enrichment factor of 3.4‰. According to the conceptual model (Fig. 6) two grid cells were defined. One grid cell corresponds to the Cr(VI) depletion zone and one to the bulk Cr(VI) solution. The initial size of the Cr(VI) depletion zone is not known. The initial volume of the Cr(VI) depletion zone was, therefore, calculated based on an arbitrary assumption that Fe(II) injected during the first minute is completely consumed by Cr(VI) reduction. This assumption resulted in a volume of 2.48 mL for the depletion zone and a volume of 197.5 mL for the bulk solution (Table 5) taking into account initial bulk Cr(VI) concentration, Fe(II) concentration of the added Fe(II) solution and the stoichiometry of the Cr(VI) reduction reaction considered by the reaction network (Eqs. (4) and (5)). The composition of the initial bulk Cr(VI) solution was specified according to Dossing et al. (2011) (Table 5). Dilute deionized water was assumed for the initial concentration of the Cr(VI) depletion zone. The injection of the Fe(II) solution was simulated by specifying 0.025 mmol of a hypothetical solid $FeCl_2$ phase within the Cr(VI) depletion zone. $FeCl_2$ was defined to kinetically dissolve following a TST rate law similar to Eq. (9) and producing aqueous Fe^{2+} and Cl^-:

$$FeCl_2 = Fe^{2+} + 2Cl^-. \tag{13}$$

An arbitrary high equilibrium constant of log(K) = 50, a reaction rate of 0.18 mmol/s/$kg_{H_2O,}$ and no surface area dependence was defined to ensure the same constant Fe(II) injection rate as in the actual experiment (0.8 mL/min, Fe(II) concentration = 35.81 mmol/L). The specification of chemical equilibrium with a hypothetical "fix_pH" mineral phase

$$fix_pH = H^+ \tag{14}$$

maintained the pH value of the bulk solution at 8.1 (Fig. 7) when using a log(K) of −8.1. In doing so, the model does not have to explicitly

Table 5
Initial conditions of the two domains defined to model the Dossing et al (2011) Fe(II)-added–Cr(VI) reduction experiment.

		Cr(VI) Bulk solution	Cr(VI) depletion zone
Volume[a]	mL	197.5	24.8
Mineralogy[a]		No mineral reaction allowed	50 vol.% NaOH, 50 vol.% $FeCl_2$, $Fe(OH)_3$ and $Cr(OH)_3$ precipitation (Cr(VI) reduction) allowed
Porosity[a]	–	1	0.1
Permeability	m[b]	1.00E−10	1.00E−10
Distance to interface	m	2.25	2.5
Initial area A between cells	m[b]	0.4	0.4
pH		8.1	7
$^{53}CrO_4^{2-}$	mol/L	3.65E−04	1.00E−10
$^{52}CrO_4^{2-}$	mol/L	3.22E−03	1.00E−10
K^+	mol/L	7.18E−03	1.00E−10
Cl^-	mol/L	6.60E−05	1.00E−10
Fe^{2+}	mol/L	1.00E−10	1.00E−10

[a] This definition leads to a initial volume of the Cr(VI) depletion zone of 2.48 mL (1.2‰ of total volume) and initial NaOH and $FeCl_2$ concentrations of 0.025 mmol and 0.08 mmol.
[b] $\delta^{53}Cr = 0.0‰$.

Author's personal copy

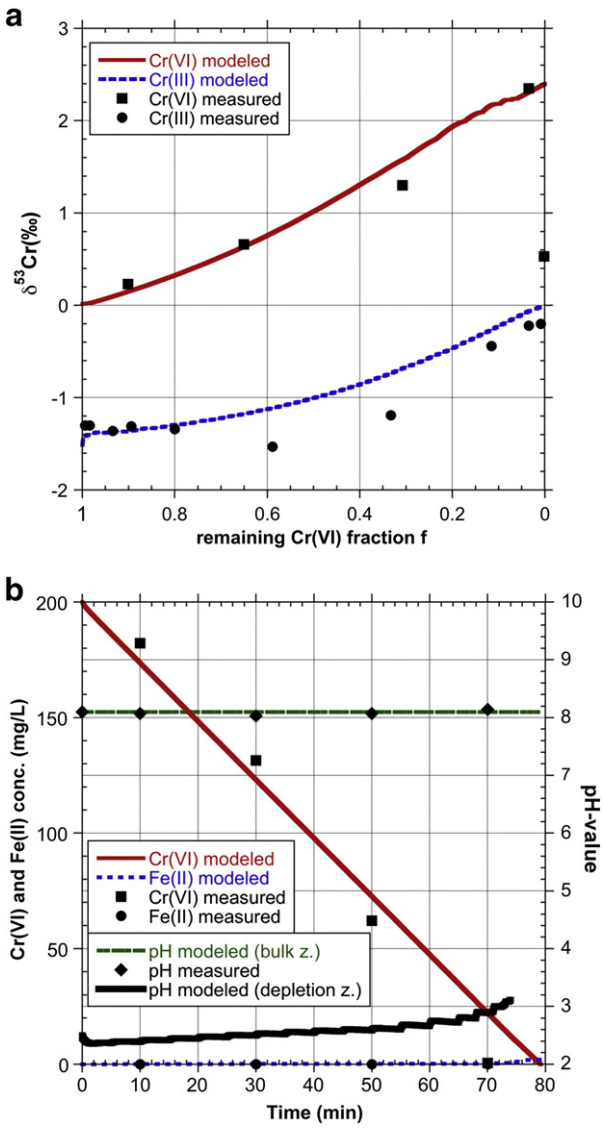

Fig. 7. Comparison between measured and modeled δ^{53}Cr-values (a) and aqueous concentrations (b) of the Dossing et al. (2011) Fe(II)-added–Cr(VI) reduction experiment. Simulated values refer to the bulk solution except for the solid δ^{53}Cr values, which refer to the Cr(VI) depletion zone, and the pH values that are shown for both zones.

consider the injection of a NaOH solution as it was performed during the Dossing et al. (2011) experiment to fix the pH at this value. Diffusive Cr(VI) transport into the depletion zone was simulated based on Eqs. (2) and (3). Small assumed values of 0.25 and 0.225 mm were assigned to d_1 and d_2, respectively (Table 5). The reaction rate constant k for the Cr(VI) reduction (Eqs. (4) and (5)) and the interfacial area between the two grid cells were calibrated in order to get an initial δ^{53}Cr of the Cr(III) formed within the depletion zone of −1.4‰ (Fig. 7). This resulted in $k = 2 \cdot 10^{-5}$ mol/m^2/s and A = 0.4 m^2. It has to be pointed out that resulting δ^{53}Cr values were only sensitive with respect to A unless k was higher than $k = 2 \cdot 10^{-20}$ mol/m^2/s. The specified diffusive flux was most likely higher than in the actual experiment because stirring effects cannot be accurately simulated with TOUGHREACT and had to be compensated by an increased diffusive flux. Furthermore, our simulations did not allow for changing grid cell volumes during a simulation run. The lack of an evolving Cr(VI) depletion zone was compensated by a time-dependent increase in the diffusive Cr(VI) flux J_D. Stopping and restarting the simulation 18 times ensured such an increase in the diffusive Cr(VI) flux because before each restart the interfacial area A (Eq. (3)) between the two zones was increased. The actual values for A (Table 6) were calibrated in order to get a good fit with the measured δ^{53}Cr values for Cr(III) and Cr(VI) respectively (Fig. 7a). Fig. 7b illustrates that the model setup and model calibration also results in a reasonable independent reproduction of measured Fe(II) and Cr(VI) concentrations as well as measured pH-values. Fig. 7b also illustrates that Cr(VI) reduction and subsequent precipitation of $Fe(OH)_3$ lead to initially low pH values within the Cr(VI) depletion zone (pH = 2.3) that only slightly increased during the course of the experiment. The observed minor pH oscillations (Fig. 7b) are a result of the stepwise increase of the interfacial area A (Table 6) leading to unsmooth OH^- diffusion into the Cr(VI) depletion zone.

3.3. Discussion

The successful simulation of the trend of all measured parameters (Fig. 7) lends strong support for our conceptual model (Fig. 6) even though the actual Cr(VI) reduction mechanism and equilibrium enrichment factor, respectively are not known and transport processes (e.g., stirring effects, evolving volumes) could not be fully simulated. The use of an increasing interface area as proxy for the evolving Cr(VI) depletion volume (Table 6) can be justified by the fact that the interfacial area must have increased as the volume of the Cr(VI) depletion zone also increased (Fig. 6). Because the interfacial area A and the reaction rate constant k were the most sensitive parameters in model calibration, it is inferred that the experiment ran in the transport and surface reaction limited regime (DePaolo, 2011), where ε_{kin} is most effectively shifted to low values (Figs. 3 and 4). Accordingly, it is suggested that the low observed enrichment factor is most likely attributed to both, a transport-limited overall Cr(VI) reduction rate and a high molecular-scale Cr(VI) reduction rate r_n. Such a fast reduction rate was possibly induced by the low pH value of the proposed Cr(VI) depletion zone since fast reaction kinetics between Cr(VI) and Fe(II) have been observed for pH values<3 (Buerge and Hug, 1997). However, the model does not explicitly consider a pH dependence on the molecular scale Cr(VI) reduction rate and it is therefore only inferred that a fast molecular-scale Cr(VI) reduction rate is necessary to obtain the observed Cr isotope fractionation. Our interpretation does not rule out contribution of another Cr(VI) reduction mechanism with a low equilibrium enrichment factor, such as stated by Dossing et al. (2011). However, a specific mechanism solely responsible for the small enrichment factor seems very unlikely since the observed value is smaller than in most other published experiments (Table 1). This observation is notable because

Table 6
Calibrated time dependent interfacial areas between the Cr(VI) depletion zone and the bulk Cr(VI) solution.

Time period (min)	Interfacial area A (m^2)
0–2	0.4
2–5	0.42
5–10	0.45
10–15	0.49
15–20	0.534
20–25	0.581
25–30	0.633
30–35	0.689
35–40	0.75
40–45	0.817
45–50	0.889
50–55	0.966
55–60	1.115
60–65	1.400
65–68	1.700
68–71	2.150
71–73	2.800
73–74	4.000
74–80	[a]

[a] Not simulated, values shown in Fig. 7 were extrapolated.

Author's personal copy

these other experiments were performed in closed systems that were much closer to equilibrium conditions than the Dossing et al. (2011) Fe(II)-added–Cr(VI) reduction experiment.

4. Conclusions

The simulations presented in this paper illustrate that a system's effective kinetic Cr isotope enrichment factor is dependent on the specific Cr(VI) reduction mechanism (e.g., equilibrium enrichment factor), specific molecular scale Cr(VI) reduction rate and on transport limitations of a system's overall Cr(VI) reduction rate. The simulations also confirmed that for surface reaction-controlled and transport-limited systems the observed effective kinetic Cr isotope enrichment factor could be substantially shifted to very low values even though the molecular scale Cr(VI) reduction mechanism remained constant. Both effects should be addressed when discussing experimental results of Cr(VI) reduction experiments but also when referring to Cr isotope data collected at field sites. In the case of the Dossing et al. experiment, a completely different interpretation could be given by addressing transport limitations and surface kinetic effects.

The fact that the proposed reaction network allowed an independent assessment of the contributions of the individual factors on the resulting enrichment factor confirms that reactive transport modeling is a powerful tool when it comes to data interpretation. Such models do, however, require a lot of quantitative information on the relevant reactive and transport processes, and many details regarding the experimental conditions. Regarding fractionation effects of different Cr(VI) reduction mechanisms, there is currently still a lack of information. An equilibrium enrichment behavior, that is a thermodynamically defined variable for a specific molecular scale Cr(VI) reduction mechanism, was so far only reported for one particular experiment. In order to have a better constraint on the degree of variation of equilibrium Cr isotopic enrichment factors, more experimental data are needed. Moreover, there is a need for more rigorous quantitative assessment of diffusive Cr(VI) transport across passivation layers and biofilms/biological reaction systems. In conjunction with reactive transport modeling such experimental data could help to tightly constrain the Cr isotope fractionation factor for a given reaction mechanism under specific experimental (e.g., transport-limited) conditions. Tightly constrained fractionation factors may then be used in conjunction with large-scale 2D or 3D reactive transport models to obtain a more robust quantification of Cr(VI) reduction efficiencies for environmental systems, and in paleoclimatic interpretations. Such models benefit from the fact that large-scale aquifer heterogeneities can be considered as well. This is important since field-scale Cr(VI) reduction mostly occurs within locally reduced domains (e.g., engineered or naturally occurring) that may be physically separated from the predominant advective contaminant transport domain. Accordingly, transport of Cr(VI) to potential reducing agents or vice versa may introduce another degree of transport limitation in addition to the ones occurring at the experimental/reaction scale.

Acknowledgments

This work was supported by the Subsurface Science Scientific Focus Area funded by the U.S. Department of Energy, Office of Science, Office of Biological and Environmental Research under award number DE-AC02-05CH11231. We thank Nicolas Spycher for constructive discussion. The manuscript was also improved thanks to the comments of two anonymous reviewers.

References

Ball, J.W., Nordstrom, D.K., 1998. Critical evaluation and selection of standard state thermodynamic properties for chromium metal and its aqueous ions, hydrolysis species, oxides, and hydroxides. Journal of Chemical and Engineering Data 43, 895–918.

Basu, A., Johnson, T.M., 2012. Determination of hexavalent chromium reduction using Cr stable isotopes: isotopic fractionation factors for permeable reactive barrier materials. Environmental Science and Technology 46, 5353–5360.

Bender, M.L., 1990. The $\delta^{18}O$ of dissolved O_2 in seawater — a unique tracer of circulation and respiration in the deep sea. Journal of Geophysical Research—Oceans 95, 22243–22252.

Berna, E.C., Johnson, T.M., Makdisi, R.S., Basui, A., 2010. Cr stable isotopes as indicators of Cr(VI) reduction in groundwater: a detailed time-series study of a point-source plume. Environmental Science and Technology 44, 1043–1048.

Bigeleisen, J., Mayer, M.G., 1947. Calculation of equilibrium constants for isotopic exchange reactions. Journal of Chemical Physics 15, 261–267.

Brandes, J.A., Devol, A.H., 1997. Isotopic fractionation of oxygen and nitrogen in coastal marine sediments. Geochimica et Cosmochimica Acta 61, 1793–1801.

Buerge, I.J., Hug, S.J., 1997. Kinetics and pH dependence of chromium(VI) reduction by iron(II). Environmental Science and Technology 31, 1426–1432.

Canfield, D.E., 2001. Biogeochemistry of sulfur isotopes. Stable Isotope Geochemistry: In: Valley, J.W., Cole, D.R. (Eds.), Reviews in Mineralogy and Geochemistry, 43, pp. 607–636.

Coby, A.J., Picardal, F., Shelobolina, E., Xu, H., Roden, E.E., 2011. Repeated anaerobic microbial redox cycling of iron. Applied and Environmental Microbiology 77, 6036–6042.

Davis, A., Olsen, R.L., 1995. The geochemistry of chromium migration and remediation in the subsurface. Ground Water 33, 759–768.

DePaolo, D.J., 2011. Surface kinetic model for isotopic and trace element fractionation during precipitation of calcite from aqueous solutions. Geochimica et Cosmochimica Acta 75, 1039–1056.

Dossing, L.N., Dideriksen, K., Stipp, S.L.S., Frei, R., 2011. Reduction of hexavalent chromium by ferrous iron: a process of chromium isotope fractionation and its relevance to natural environments. Chemical Geology 285, 157–166.

Dzombak, D.A., Morel, F.M.M., 1990. Surface Complexation Modeling: Hydrous Ferric Oxide. John Wiley & Sons, New York.

Ellis, A.S., Johnson, T.M., Bullen, T.D., 2002. Chromium isotopes and the fate of hexavalent chromium in the environment. Science 295, 2060–2062.

Faybishenko, B., Hazen, T.C., Long, P.E., Brodie, E.L., Conrad, M.E., Hubbard, S.S., Christensen, J.N., Joyner, D., Borglin, S.E., Chakraborty, R., Williams, K.H., Peterson, J.E., Chen, J., Brown, S.T., Tokunaga, T.K., Wan, J., Firestone, M., Newcomer, D.R., Resch, C.T., Cantrell, K.J., Willett, A., Koenigsberg, S., 2008. In situ long-term reductive bioimmobilization of Cr(VI) in groundwater using hydrogen release compound. Environmental Science and Technology 42, 8478–8485.

Flury, B., Eggenberger, U., Mäder, U., 2009. First results of operating and monitoring an innovative design of a permeable reactive barrier for the remediation of chromate contaminated groundwater. Applied Geochemistry 24, 687–696.

Frei, R., Gaucher, C., Poulton, S.W., Canfield, D.E., 2009. Fluctuations in Precambrian atmospheric oxygenation recorded by chromium isotopes. Nature 461, 250-U125.

Frost, R.L., 2004. Raman microscopy of selected chromate minerals. Journal of Raman Specroscopy 35, 153–158.

Green, C.T., Bohlke, J.K., Bekins, B.A., Phillips, S.P., 2010. Mixing effects on apparent reaction rates and isotope fractionation during denitrification in a heterogeneous aquifer. Water Resources Research 46.

Han, R., Geller, J.T., Yang, L., Brodie, E.L., Chakraborty, R., Larsen, J.T., Beller, H.R., 2010. Physiological and transcriptional studies of Cr(VI) reduction under aerobic and denitrifying conditions by an aquifer-derived pseudomonad. Environmental Science and Technology 44, 7491–7497.

Han, R., Qin, L., Brown, S.T., Christensen, J.N., Beller, H.R., 2012. Differential isotopic fractionation during Cr(VI) reduction by an aquifer-derived bacterium under aerobic versus denitrifying conditions. Applied and Environmental Microbiology 78, 2462–2464.

Hancock, R.E.W., Wong, P.G.W., 1984. Compounds which increase the permeability of the *Pseudomonas aeruginosa* outer-membrane. Antimicrobial Agents and Chemotherapy 26, 48–52.

Harvey, R.W., George, L.H., Smith, R.L., Leblanc, D.R., 1989. Transport of microspheres and indigenous bacteria through a sandy aquifer: results of natural- and forced-gradient tracer experiments. Environmental Science and Technology 23, 51–56.

Izbicki, J.A., Ball, J.W., Bullen, T.D., Sutley, S.J., 2008. Chromium, chromium isotopes and selected trace elements, western Mojave Desert, USA. Applied Geochemistry 23, 1325–1352.

Jamieson-Hanes, J.H., Gibson, B.D., Lindsay, M.B.J., Kim, Y., Ptacek, C.J., Blowes, D.W., 2012. Chromium isotope fractionation during reduction of Cr(VI) under saturated flow conditions. Environmental Science and Technology 46, 6783–6789.

Jeen, S.W., Jambor, J.L., Blowes, D.W., Gillham, R.W., 2007. Precipitates on granular iron in solutions containing calcium carbonate with trichloroethene and hexavalent chromium. Environmental Science and Technology 41, 1989–1994.

Johnson, J.W., Oelkers, E.H., Helgeson, H.C., 1992. SUPCRT92: a software package for calculating the standard molal thermodynamic properties of minerals, gases, aqueous species, and reactions from 1 to 5000 bar and 0 to 1000 °C. Computer & Geoscience 18, 899–948.

Jones, C.M., Niederweis, M., 2010. Role of porins in iron uptake by *Mycobacterium smegmatis*. Journal of Bacteriology 192, 6411–6417.

Kitchen, J.W., Johnson, T.M., Bullen, T.D., Zhu, J., Raddatz, A., 2012. Chromium isotope fractionation factors for reduction of Cr(VI) by aqueous Fe(II) and organic molecules. Geochimica et Cosmochimica Acta 89, 190–201.

Kotas, J., Stasicka, Z., 2000. Chromium occurrence in the environment and methods of its speciation. Environmental Pollution 107, 263–283.

Lasaga, A.C., 1984. Chemical kinetics of water–rock interactions. Journal of Geophysical Research 89, 4009–4025.

Nikaido, H., 2003. Molecular basis of bacterial outer membrane permeability revisited. Microbiology and Molecular Biology Reviews 67, 593–656.

Nordstrom, D.K., Munoz, J.L., 1985. Geochemical Thermodynamics. Benjamin/Cummings Publishing Company, Redwood City, CA USA.

Author's personal copy

Palmer, C.D., Puls, R.W., 1994. Natural attenuation of hexavalent chromium in groundwater and soils. EPA Ground Water Issue Paper EPA/540/5-94/505. U.S. Environmental Protection Agency, U.S Government Printing Office, Washington, DC.

Pearson, J.P., Van Delden, C., Iglewski, B.H., 1999. Active efflux and diffusion are involved in transport of *Pseudomonas aeruginosa* cell-to-cell signals. Journal of Bacteriology 181, 1203–1210.

Rai, D., Sass, B.M., Moore, D.A., 1987. Chromium(III) hydrolysis constants and solubility of chromium(III) hydroxide. Inorganic Chemistry 26, 345–349.

Reed, M.H., 1982. Calculation of multicomponent chemical equilibria and reaction processes in systems involving minerals, gases and aqueous phase. Geochimica et Cosmochimica Acta 46, 513–528.

Rees, C.E., 1973. Steady-state model for sulfur isotope fractionation in bacterial reduction processes. Geochimica et Cosmochimica Acta 37, 1141–1162.

Schauble, E., Rossman, G.R., Taylor, H.P., 2004. Theoretical estimates of equilibrium chromium-isotope fractionations. Chemical Geology 205, 99–114.

Schoenberg, R., Zink, S., Staubwasser, M., von Blanckenburg, F., 2008. The stable Cr isotope inventory of solid earth reservoirs determined by double spike MC-ICP-MS. Chemical Geology 249, 294–306.

Sikora, E.R., Johnson, T.M., Bullen, T.D., 2008. Microbial mass-dependent fractionation of chromium isotopes. Geochimica et Cosmochimica Acta 72, 3631–3641.

Singleton, M.J., Sonnenthal, E.L., Conrad, M.E., DePaolo, D.J., Gee, G.W., 2004. Multiphase reactive transport modeling of stable isotope fractionation in unsaturated zone pore water and vapor: application to seasonal infiltration events at the Hanford Site, WA. Vadose Zone Journal 3, 775–785.

Urey, H.C., 1947. The thermodynamic properties of isotopic substances. Journal of the Chemical Society 562–581.

Wanner, C., Eggenberger, Mäder, U., 2011. Reactive transport modeling of Cr(VI) treatment under fast flow conditions. Applied Geochemistry 26, 1513–1523.

Wanner, C., Eggenberger, U., Kurz, D., Zink, S., Mäder, U., 2012a. A chromate-contaminated site in southern Switzerland, part 1: site characterization and the use of Cr isotopes to delineate fate and transport. Applied Geochemistry 27, 644–654.

Wanner, C., Zink, S., Eggenberger, U., Mäder, U., 2012b. Assessing the Cr(VI) reduction efficiency of a permeable reactive barrier using Cr isotope measurements and 2D reactive transport modeling. Journal of Contaminant Hydrology 131, 54–63.

Wanner, C., Eggenberger, Mäder, U., 2012c. A chromate-contaminated site in southern Switzerland, part 2: reactive transport modeling to optimize remediation options. Applied Geochemistry 27, 655–662.

Watson, E.B., Mueller, T., 2009. Non-equilibrium isotopic and elemental fractionation during diffusion-controlled crystal growth under static and dynamic conditions. Chemical Geology 267, 111–124.

Wolery, T.J., 1992. EQ3/6: software package for geochemical modeling of aqueous systems: package overview and installation guide (version 7.0). Lawrence Livermore National Laboratory Report UCRL-MA-110662 PT I. Livermore, California.

Xu, T., 2008. Incorporating aqueous reaction kinetics and biodegradation into TOUGHREACT: applying a multiregion model to hydrobiogeochemical transport of denitrification and sulfate reduction. Vadose Zone Journal 7, 305–315.

Xu, T., Spycher, N.F., Sonnenthal, E., Zhang, G., Zheng, L., Pruess, K., 2011. TOUGHREACT version 2.0: a simulator for subsurface reactive transport under non-isothermal multiphase flow conditions. Computer & Geoscience 37, 763–774.

Young, E.D., Galy, A., Nagahara, H., 2002. Kinetic and equilibrium mass-dependent isotope fractionation laws in nature and their geochemical and cosmochemical significance. Geochimica et Cosmochimica Acta 66, 1095–1104.

Zink, S., Schoenberg, R., Staubwasser, M., 2010. Isotopic fractionation and reaction kinetics between Cr(III) and Cr(VI) in aqueous media. Geochimica et Cosmochimica Acta 74, 5729–5745.